Synthesis, structure and electrochemical performance of the argyrodite Li_6PS_5Cl solid electrolyte for Li-ion solid state batteries

Yu, Chuang; van Eijck, Lambert; Ganapathy, Swapna; Wagemaker, Marnix

DOI
10.1016/j.electacta.2016.08.081

Publication date
2016

Document Version
Final published version

Published in
Electrochimica Acta

Electrochimica Acta 215 (2016) 93–99

Contents lists available at ScienceDirect

Electrochimica Acta

journal homepage: www.elsevier.com/locate/electacta

Synthesis, structure and electrochemical performance of the argyrodite Li_6PS_5Cl solid electrolyte for Li-ion solid state batteries

Chuang Yu, Lambert van Eijck, Swapna Ganapathy, Marnix Wagemaker*

Department of Radiation Science and Technology, Delft University of Technology, Mekelweg 15, Delft 2629JB, The Netherlands

ARTICLE INFO

Article history:
Received 17 May 2016
Received in revised form 16 August 2016
Accepted 17 August 2016
Available online 18 August 2016

Keywords:
Li-ion batteries
solid state batteries
Argyrodite Li6PS5Cl
solid electrolytes
Li-ion conduction

ABSTRACT

The high lithium conductivity of argyrodite Li_6PS_5Cl makes it an attractive candidate as solid electrolyte in all solid-state Li batteries. Aiming at an optimal preparation strategy the structure and conductivity upon different mechanical milling times is investigated. Li_6PS_5Cl material with high ionic conductivity of $1.1{\cdot}10^{-3}$ S/cm was obtained by milling for 8 hours at 550 rpm followed by a heat-treatment at 550 °C. All solid-state Li-S batteries were assembled, combining the Li_6PS_5Cl solid electrolyte, with a carbon-sulfur mixture as positive electrode and Li, Li-Al and Li-In as negative electrode. An optimum charge/discharge voltage window between 0.4 and 3.0 V vs. Li-In was obtained by CV experiments and galvanostatic cycling displays a very large capacity around 1400 mAh/g during the first cycles, decreasing below 400 mAh/g after 20 cycles. Impedance spectroscopy suggests that the origin of the capacity fading is related to an increasing electrode-electrolyte interface resistance.

1. Introduction

The demand for safe electrical energy storage technologies with high energy density for electric vehicle applications is emerging [1]. Li-ion batteries with organic liquid electrolytes have safety issues due to potential electrolyte leakage and the inherent flammability [2]. Unlike liquid electrolytes, solid electrolytes are non-flammable mitigating most safety issues and in addition the reduced packaging demands potentially improves the gravimetric and volumetric energy density. However, one of the biggest obstacles for the commercial applicability of solid electrolytes in all solid state batteries is their low ionic conductivity compared to conventional organic liquid electrolytes [2].

Numerous efforts have been devoted to finding solid Li-ion conductors with high ionic conductivities, a wide electrochemical stability window and excellent chemical stability. For practical battery application the conductivity of the solid electrolyte needs to exceed 10^{-3} S/cm near room temperature. Intensive research has led to several families of electrolytes, including the sulphides (Li_2S-P_2S_5, Li_2S-SiS_2, Li_2S-GeS_2) [3,4], the oxides ($Li_7La_3Zr_2O_{12}$ and $Li_{3x}La_{2/3-3x}TiO_3$) [5,6] and the phosphates (LiPON, $Li_{1+x}Al_xGe_{2-x}(PO_4)_3$, $Li_{1+x}Ti_{2-x}Al_x(PO_4)_3$) [7–9]. Among them, oxides and phosphates display relatively small low ionic conductivities, mainly attributed to the high grain boundary resistances [2]. More recently there has been a renewed interest in $Li_{10}GeP_2S_{12}$, having a very high ionic conductivity of 10^{-2} S/cm at room temperature [10]. However, the large costs of the GeS_2 starting material required for its synthesis limits its potential for large scale applications. Another important emerging family of solid electrolytes are the Li-argyrodites Li_6PS_5X (X = Cl, Br and I) with Li-ion conductivities in the range of 10^{-2}–10^{-3} S/cm at room temperature [11]. In addition to high Li-ion conductivities Li_6PS_5Cl is reported to have a wide electrochemical window up to 7.0 V vs. Li/Li^+ [12]. The conductivities of these materials are comparable to $Li_{10}GeP_2S_{12}$, however the much cheaper precursors gives this family of materials a large potential to be applied in all solid state batteries. Sylvain et al. [12,13] assembled solid state cells using Li_6PS_5Cl as the electrolyte, $LiCoO_2$ as the cathode, and spinel $Li_4Ti_5O_{12}$ as anode, exhibiting excellent electrochemical performance. The theoretical capacity of $LiCoO_2$ however is relatively small motivating research on high capacity electrode materials. Sulphur has attracted much attention in past years because of its high theoretical capacity of 1672mAh/g, giving a theoretical specific energy of 2500 Wh/kg, making it one of the most promising anode materials for next generation lithium batteries [14]. However, Li-ion batteries with sulphur in combination with a liquid electrolyte has many problems including short cycle life, low charging efficiency, poor safety, and a high self-discharge rate, all of which are related to the dissolution of lithium polysulfide, the series sulphur reduction intermediates in liquid electrolyte and resulting

* Corresponding author.
E-mail address: m.wagemaker@tudelft.nl (M. Wagemaker).

http://dx.doi.org/10.1016/j.electacta.2016.08.081
0013-4686/

parasitic reactions [15–17]. By combining sulphur with solid electrolytes, such as Li_3PS_4 [18] and Li_2S-P_2S_5 [19], the high capacities of sulphur may be better utilised, making this a promising system for future applications. Chen et al. [20] combined S with Li_6PS_5Br to construct a solid-state cell, showing an initial discharge capacity of 1355mAh/g and reversible capacity of 1080 mAh/g after 50 cycles. They attributed the excellent electrochemical performance of the solid-state battery to the small particle size of the active materials.

Rao *et al.* [21] reported on the synthesis protocols for argyrodite Li_6PS_5X (X = Cl, Br, I) using high speed mechanical milling followed by an annealing treatment, resulting in crystalline materials with Li-ion conductivities on the order of 10^{-3} S/cm at room temperature. Using neutron powder diffraction during annealing Rao et al. [22] were able to establish a clear correlation between the annealing temperature and the ionic conductivity. It was concluded that an annealing temperature of at least 250 °C is required to obtain ionic conductivities reaching 10^{-3} S/cm. [22] With combined refinement of XRD and Neutron Diffraction patterns Rayavarapy et al. [23] showed that besides the disorder in the lithium distribution the disorder in the S^2/Cl^- or $S^2//Br^-$ distribution promotes the Li-ion mobility, also supported by recent bond-valence analysis calculations [24]. Various studies have been performed to obtain the ionic in Li_6PS_5X (X = Cl, Br, I) using impedance spectroscopy [11,12,21–23,25,26] resulting in conductivities varying between 10^{-7} and 10^{-2} S/cm and activation energies varying between 0.11 and 0.56 eV.

By considering the structure and conductivity depending as a function of the ball mill synthesis route the present work aims at an optimal synthesis route of Li_6PS_5Cl. Batteries combining Li_2S as positive electrode, Li_6PS_5Cl as electrolyte and In as negative electrode were assembled to determine the optimal dis(charge) window, resulting in high initial capacities approaching 1500 mAh/g degrading over 20 cycles towards 400 mAh/g.

2. Experimental

Reagent-grade Li_2S (99.98%, Sigma-Aldrich), P_2S_5 (99%, Sigma-Aldrich), and LiCl (99.0%, Sigma-Aldrich) crystalline powders were used as starting materials. The required amount of starting materials were ball milled in a WC coated (inner) stainless steel jar with 10 WC balls (8 g/ball) in an Argon filled glovebox (H_2O, $O_2 < 0.3$ ppm) because of the reactivity with oxygen and moisture. The total weight of the mixture was almost 2.0 grams, and the ball milling speed was fixed at 550 rpm. The milling duration was varied to find the optimal milling time. After subsequent mixing times a small amount of powder was collected to perform powder XRD. After the ball milling process, the mixture was sealed in a quartz tube and annealed at 550 °C for 5 hours to obtain the final Li_6PS_5Cl solid electrolyte.

Powder XRD patterns were collected over a 2θ range of 10-160° to identify the crystalline phases of the prepared materials using $Cu_{K\alpha}$ X-rays (1.5406 Å at 45 kV and 40 mA) on an X'Pert Pro X-ray diffractometer (PANalytical). To prevent reaction with moisture and oxygen the powders were sealed in an airtight XRD sample holder in an Argon filled glove box.

The neutron data were collected on the new neutron powder diffractometer PEARL of the TU Delft [27]. Data were collected at room temperature using the (533) reflection of the germanium monochromator (lambda = 1.665AA). The sample was loaded under Argon in a 6 mm diameter air-tight vanadium sample can. The sample was measured for 18 hours from 10.4–160 degrees 2θ. The sample can is under vacuum during the data collection. The data treatment consisted of a relative correction for detection efficiency of (each of) the 1408 detector pixels and a substraction of the background, caused by the instrument and the sample can. Rietveld refinement was performed using GSAS [28].

Ionic conductivities of the ball-milled powders and the final Li_6PS_5Cl solid electrolyte were measured by preparing pallets of the powder with a diameter of 10 mm. Stainless-steel disks were attached on both faces of the pellets. AC impedance measurements were performed on an Autolab (Autolab PGSTAT302N) in the frequency range of 0.1 Hz to 1 MHz with an applied voltage of 0.05 V.

Laboratory-scale solid-state Li-S batteries were fabricated in the following manner: The S-C composite was obtained firstly by mixing S at 450 rpm for 6 h, Active carbon (Super P, TIMCAL) was added with a weight ratio of 1:1, and the composite was mixed at 500 rpm for 3 h. After that, the ball-milled S-C mixture was sealed in a quartz tube and annealed at 155 °C for 12 h [29]. Finally, the obtained S-C composite was mixed with Li_6PS_5Cl and super P with a weight ratio of 4:4:2 and a rotation speed of 450 rpm for 1 h. Then, a two-layer pellet (d = 10 mm), consisting of 12 mg of the described cathode mixture and 88 mg Li_6PS_5Cl solid electrolyte was pressed together using 6 tons of pressure. After that, a piece of Li-In alloy foil (or Li metal, Li-Al alloy) was attached on the other side, this triple-pellet was pressed with 2 tons of pressure for 30 s. The Li-In and Li-Al electrodes were obtained by pressing a piece of Li metal (ϕ = 8 mm) and a piece of In or Al foil (ϕ = 6 mm) together. The assembled cell was charged and discharged under a current density of 0.064 mA/cm^2 between 0.4 and 3.0 V to evaluate the electrochemical performance. The test cell was cathode-limited, which means that there was a lithium excess in the Li-In alloy anode. The obtained capacity was normalized by the weight of S in the cathode electrode. The CV measurements of the solid-state battery were performed at different voltage windows with a sweep speed of 0.5 mV/s. The EIS measurements were conducted with an Autolab (Autolab PGSTAT302N) before and after the charge/discharge process in the frequency range of 0.1 Hz and 1 MHz with an applied voltage of 0.05 V.

3. Results and discussions

Fig. 1 shows XRD patterns for the mixture prepared by mechanically milling Li_2S, P_2S_5 and LiCl powders between 1 to 16 h. The raw materials were mixed and ball milled at 110 rpm for 1 h to get a homogenous mixture. The reflections of the mixture

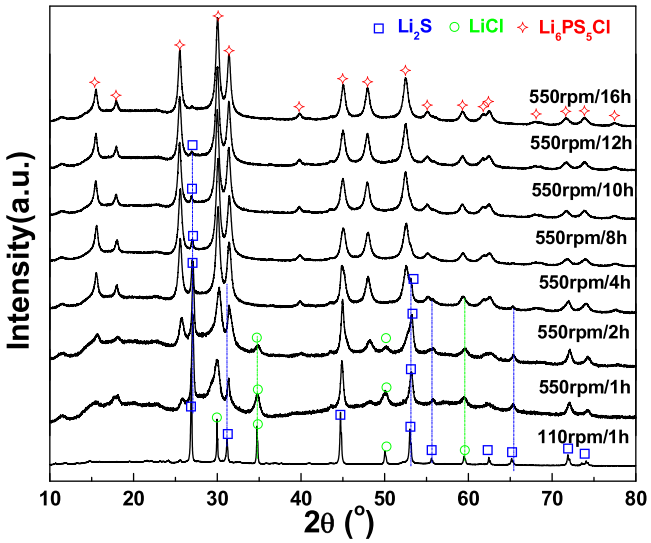

Fig. 1. XRD patterns of the mixture of Li_2S, P_2S_5 and LiCl powders ball milled with different milling times.

after 110 rpm are attributable to the starting materials. After that, the ball milling speed was fixed at 550 rpm and the mixture was mechanically milled with increasing durations. The intense diffraction peaks at 27°, 31°, 45°, 53°, 56°, 65°, 72° and 74° can be indexed by the Li_2S structure, while the other diffraction peaks of the pattern are attributed to LiCl. The intensity of diffraction peaks of Li_2S and LiCl gradually decrease with increasing milling durations. After 550 rpm for 4 h, the major peaks of the pattern can be indexed to the Li_6PS_5Cl crystal structure, although a small additional reflection is still visible at 27° which disappears when the milling time is 16 h. No obvious halo pattern was detected, indicating that no significant glassy phase was formed during the milling process. Therefore, the XRD patterns indicate that pure Li_6PS_5Cl was obtained directly by precipitation of the raw materials using mechanical milling. The present results show that the ionic conductivity does not improve after 8 hours of milling, which is shorter than the durations Sylvain et al. [12] reported. Interestingly, Sylvain et al. [12] report that the conductivity of the mixture decreases after an optimum milling duration of 10 hours whereas the present results show an unchanged conductivity between 8 and 16 hours of milling. A possible explanation is that during the milling process in the present work the jar was opened every hour to grind the mixture by hand to promote the homogeneity of the mixture. This may also explain the relative short milling time to obtain the Li_6PS_5Cl phase which is also much shorter than reported by Rao et al. [21], applying the same rotating speed during milling.

The above XRD results indicate that the Li_6PS_5Cl phase is formed after milling at 550 rpm for 4 h, after which the patterns remain almost unchanged. The impedance spectra, and resulting conductivities in Fig. 2 shows that the resistance of the pressed pellet decreases with increasing milling time, indicating a higher Li^+ conductivity of the mixture. As shown in Fig. 2b, the mixture displays very low ionic conductivity after milling for less than 2 hours, most likely caused by poor ionic conductivity of the starting materials. The XRD results indicate that after 1 and 2 hours milling at 550 rpm a considerable amount of Li_2S is present. Longer milling increases, the conductivity until 8 hours of milling after which the conductivity remains almost unchanged. For the present research the mixture milled for 16 h was chosen as material for further research, the Li^+ ion conductivity of which is 1.0×10^{-3} S/cm. To improve the conductive property this material was annealed at 550 °C for 5 h to improve the crystallinity and to create better grain boundary contact between the Li_6PS_5Cl particles. The XRD pattern of the annealed sample reflects the higher crystallinity compared to the material prepared by direct precipitation (see Supporting Information Fig. S1). Due to the annealing the Li^+ ion conductivity as measured by impedance spectroscopy increases to 1.1×10^{-3} S/cm (see Supporting Information Fig. S2), a value close that reported by Sylvain et al. [12] and Rao et al. [21] Thus heat treatment improves the crystallinity of Li_6PS_5Cl which is accompanied by an increase in Li-ion conductivity.

The X-ray powder diffraction and Neutron diffraction powder patterns of Li_6PS_5Cl (after annealing at 550 °C for 5 h) were simultaneously refined using the Rietveld method as implemented in GSAS [30,31], the patterns and fits are shown in Fig. 3. Refinement to the cubic F-43 m phase results in excellent fits, where the resulting atomic parameters are listed in Table 1. During the simultaneous Rietveld refinement of the XRD and ND patterns both the sum of the occupancies on the 4a site (S and Cl) and on the 4c sites (S and Cl) was constraint to 1 and the mean square displacement (U_{iso}) of both atoms on the same site was coupled. The occupancies on the 4b and 16e sites was not fitted and set to its stoichiometric value. The Li-ion occupancy and isotropic displacement parameter on the 48 h site was fitted without constraints. The resulting large isotropic displacement parameter reflects the high room temperature mobility of the Li-ion. The results of the Rietveld refinement in Table 1 indicate a stoichiometry of $Li_{5.6}PS_{4.8}Cl_{1.2}$, having a slightly larger degree of substitution of S with Cl, consistently leading to more charge compensated Li-ion vacancies compared to the intended Li_6PS_5Cl stoichiometry. In agreement with Rao et al. [21,22] a larger Cl occupancy is found on the Cl(1) site, with almost 60% of the Cl occupying the Cl(1) site, the resulting disorder of which appears to be a prerequisite for the high conductivity along with the crystallinity. [21]

Fig. 4 shows the XRD patterns of the pristine sulphur, sulphur-carbon composite and the mixture of Li_6PS_5Cl and sulphur-carbon composite. The diffraction peaks of the pristine sulphur and ball milled sulphur can be indexed by the orthorhombic α-S phase. Active carbon was selected based on its high BET surface. The XRD pattern of the ball milled mixture of active carbon and α-S before and after annealing at 155 °C reflect the highly amorphous nature of the mixture. The low viscosity of sulphur at 155 °C makes that it can penetrate into the channels of the active carbon. [29] Subsequent annealing most likely improves the contact of the active carbon with the sulphur, improving the conductivity of the composite. The carbon-sulphur composite and the Li_6PS_5Cl powder material were mixed and mechanically milled to form a homogenous composite cathode mixture where XRD indicates no other crystalline phases after mixing.

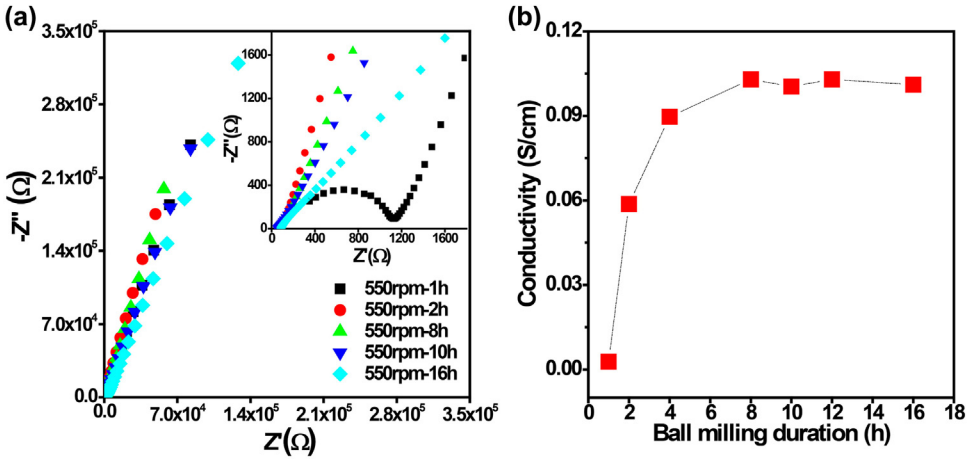

Fig. 2. (a) Complex impedance plots for the sample ball milled for different durations. The inset shows the results at small Ω (0 to 1700 Ω). (b) The conductivity of the ball-milled samples vs. the milling times.

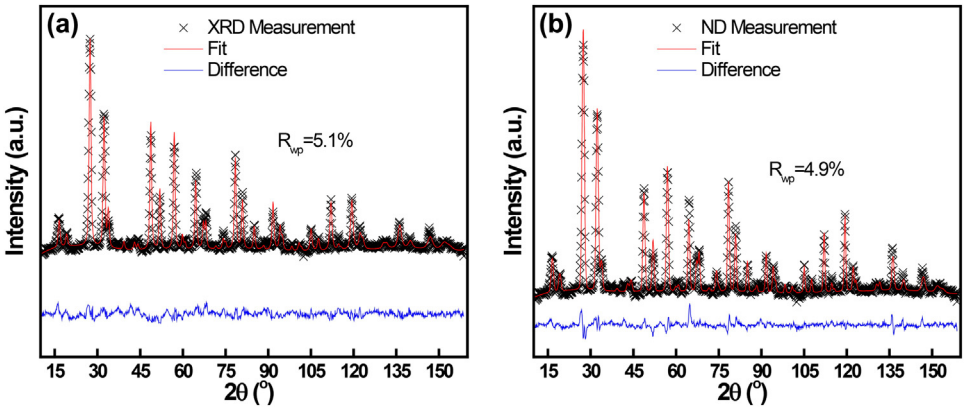

Fig. 3. (a) X-ray powder and (b) Neutron powder diffraction patterns of Li_6PS_5Cl at room temperature (after annealing at 550 °C for 5 h) simultaneously refined by Rietveld refinement.

Table 1
Lattice parameter, fractional atomic coordinates, isotropic atomic displacement parameters (U_{iso}) and site occupancies resulting from the simultaneous Rietveld refinement of cubic Li_6PS_5Cl at room temperature.

	Atom	Fractional coordinates			Wyckoff	Occupancy	U_{iso}
		X	Y	z			(Å^2)
Li_6PS_5Cl	Li	0.1766	0.1766	0.0224	48h	0.47	0.0666
F-43m	P	0. 5	0.5	0.5	4b	1.00	0.0181
a = 9.8290 Å	S(1)	0.6205	0.6205	0.6205	16e	1.00	0.0310
	S(2)	0.25	0.25	0.25	4c	0.29	0.0382
	Cl(2)	0.25	0.25	0.25	4c	0.71	0.0382
	S(3)	0.0	0.0	0.0	4a	0.48	0.0383
	Cl(1)	0.0	0.0	0.0	4a	0.52	0.0383

In solid-state cell research is typically focussed on the positive electrode and solid electrolyte combinations. For the $Li_7P_3S_{11}$ or Li_6PS_5X (X = I, Cl, Br), In is most often applied as negative electrode material most likely because of instabilities versus Li-metal. [32,33] To investigate the influence of different negative electrode materials Li metal, Li-Al alloy and Li-In were prepared in combination with the prepared Li_6PS_5Cl solid electrolyte and C-S positive electrode mixtures and cyclic voltammetry (CV) was performed. To explore the electrochemical stability of the negative electrode-electrolyte combinations and the cyclability of the solid-state cells the CV measurements were performed between different voltage sweep windows. For Li-metal as negative electrode it is observed that when the voltage exceeds 2.2 V vs. Li/Li^+ the current stabilizes with increasing voltage, Fig. S3 in the Supporting Information, indicating that the Li-Li_6PS_5Cl interface is electrochemically unstable. To verify this is indeed caused by an electrochemical reaction the chemical stability between Li metal and Li_6PS_5Cl was also investigated. Li-metal and Li_6PS_5Cl was hand ground by a mortar in an Argon glovebox, in the same weight ratio as the solid-state cell, and the mixture was subjected to XRD in an airtight holder. The diffraction peaks of the mixture are attributed to Li-metal and Li_6PS_5Cl, suggesting that Li metal is chemically stable with the Li_6PS_5Cl solid electrolyte at room temperature (Fig. S4 in the Supporting Information). This implies that the Li-Li_6PS_5Cl is electrochemically unstable above 2.2 V vs. Li/Li^+ thereby restricting the application of Li-metal in combination with Li_6PS_5Cl to low potential positive electrode materials such as spinel $Li_4Ti_5O_{12}$ and Si and excluding high potential positive electrode materials such as olivine-type, spinel-type, layered-type, S and Li_2S.

Additionally, a Li-Al alloy was used as a negative electrode where the CV tests displays no obvious cathodic and anodic peaks, Fig. S6 in the Supporting Information. The intensity of the oxidation and reduction peaks decreased dramatically with increasing cycling numbers except when setting a sweep potential window between 0.6 and 3.0 V vs. Li-Al alloy. Impedance spectroscopy of the S-C/Li_6PS_5Cl/Li-Al battery before and after the CV experiments with the best performing potential window of 0.6 and 3.0 V vs. Li-Al shows a dramatic increase in the internal resistance, Fig. S7 in the Supporting Information. Fig. 5 shows the CV curves of the solid-state S/Li_6PS_5Cl battery using the Li-In alloy as negative electrode material for 6 cycles with various potential windows at a scan rate of 0.5 mV/s. An anodic peak can be observed around 2.0 V vs Li-In, corresponding to 2.62 V vs Li/Li^+ representing the oxidation of Li_2S to lower order poly-sulphides and the cathodic peak at 0.75 V vs Li-In, corresponding to 1.35 V vs Li/Li^+ representing the reduction of S to higher order poly-sulphides. The intensity of the cathodic and anodic peaks can be attributed to the discharge and charge capacities, and the differences between the two are an indication of the cycling efficiency. From Fig. 5 it is observed that the potential window of 0.4 to 3.0 V vs. Li-In results in the best cycling performance. With increasing sweep potential window, the differences between the cathodic and anodic peak becomes larger, indicating an increasing polarization of the solid-state Li-S battery. The comparison on the impedance spectroscopy

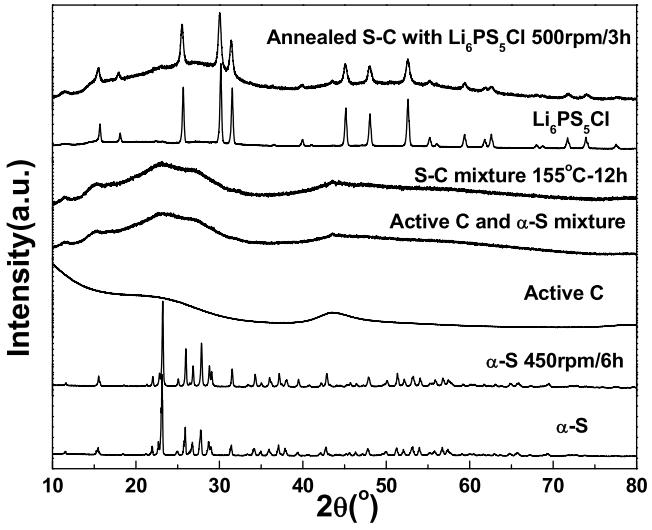

Fig. 4. XRD patterns of pristine sulphur, active C, ball-milled sulphur, S-C composite and S-C-Li_6PS_5Cl composite.

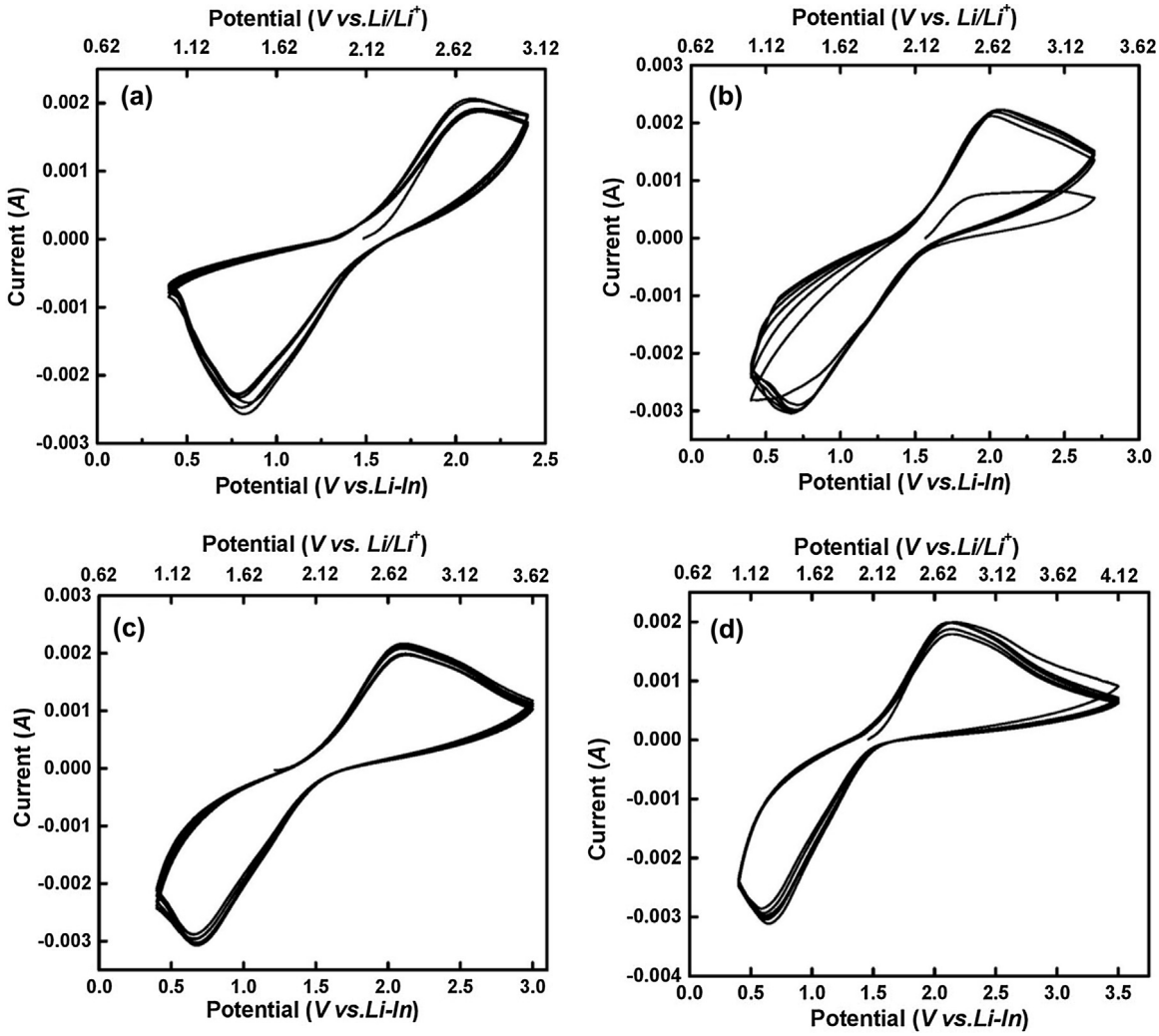

Fig. 5. The Cyclic voltammograms of the S-C/Li_6PS_5Cl/Li-In all-solid-state batteries for different voltage cut-off ranges (a) 0.4 to 2.4, (b) 2.7, (c) 3.0 and (d) 3.5 V vs. Li-In, at a scanning rate of 0.5 mV/s. The bottom voltage axis shows the values of the voltage versus Li-In, the top voltage axis shows the corresponding values of voltage versus Li/Li^+.

before and after the CV experiments in the optimal voltage window, 0.4 and 3.0 V vs Li-In, suggests that the charge transport kinetics is hardly effected by the cycling, Fig. S5 in the Supporting Information, in contrast to the Li-Al results. In combination with the battery better cycleability this indicates that Li-In performs much better as negative electrode for a solid-state battery combining Li_6PS_5Cl and S-C.

Finally, the potential for application of Li_6PS_5Cl with other common cathode materials was also investigated. (See Supporting Information Fig. S8.) Layered-type $LiNi_xMn_yCo_{1-x-y}O_{12}$ $(0<(x, y)<1)$ and its analogues were mixed with Li_6PS_5Cl and then measured with impedance spectroscopy. The mixture shows an extremely low resistance, indicating that Li_6PS_5Cl is an excellent candidate solid electrolyte by combining it with layered cathode materials in an all-solid-state cell.

To test the cycleabilty the S-C/Li_6PS_5Cl/Li-In solid state battery was galvanostatically cycled, with a current of 0.064 mA/cm^2, between the optimal potential window of 0.4 and 3.0 V vs Li-In as shown in Fig. 6. After an initial activation cycle the discharge capacities of the second and third cycles result in 1388.5 and 1459.0 mAh/g respectively, slightly below the theoretical capacity of Sulphur 1600 mAh/g [14]. The charge capacities of the second and third cycle are larger than the discharge capacities potentially indicating that the cathode mixture also participates in the electrochemical reaction during the initial cycles, which also observed by Nagao et al. [34] After the very high capacities during the first few cycles it decreases quickly in the subsequent cycles towards 389 mAh/g after 20 cycles. Comparison of the impedance spectrum between the fresh cell and after 20 cycles, shown in Fig. 6c, exhibits, two intersections with the Z' axis, R_1 at the high frequency side (left side of horizontal axis), and R_2 at the low frequency side (right side of horizontal axis) representing the resistance of the solid electrolyte and the total resistance of the solid-state cell (solid electrolyte and electrode-solid electrolyte interface) respectively. The resistance from the electrode-solid electrolyte interface part can be calculated by subtracting R_1 from R_2. [35] For the fresh solid-state cell this results in 82.7 and 4.5 Ω for the fresh cell, the corresponding values for the cell are 178.8 and 31.2 Ω after 20 cycles, for the solid electrolyte resistance and resistance of the electrode-solid electrolyte interface respectively. In particular, the large increase in the resistance of the electrode-solid electrolyte may indicate loss in contact of the electrode with the solid electrolyte due to the large changes in electrode volume of both Sulphur and Li-In.

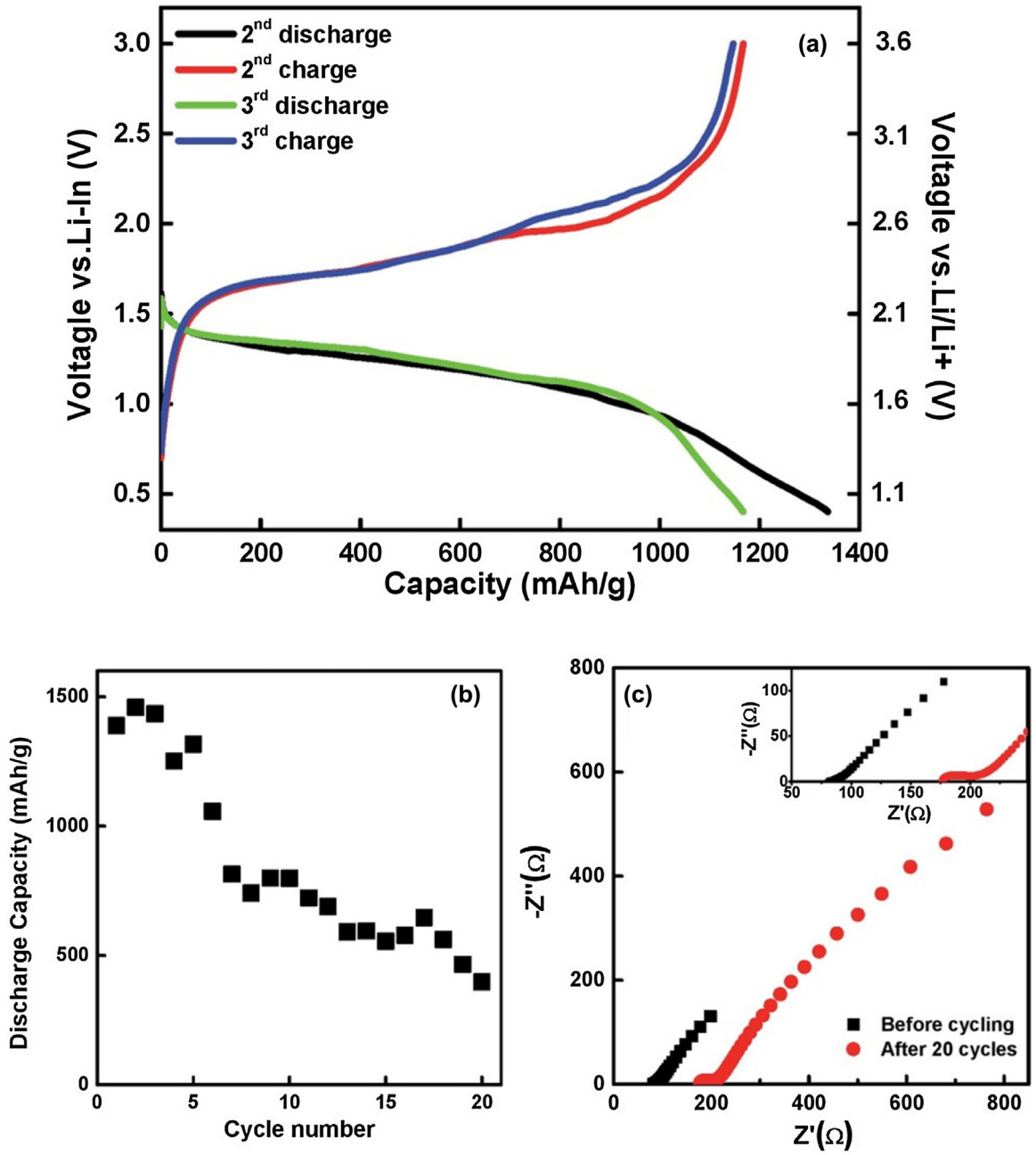

Fig. 6. a) The 2nd and 3rd charge/discharge galvanostatic voltage curves for the assembled all-solid-state C-S/Li_6PS_5Cl/Li-In battery. The initial cycle to activate the battery is not shown here. The (dis)charge current density is 0.064 mA/cm^2 and the cut-off potentials are set at 0.4 and 3.0 V vs. Li-In. b) Evolution of the capacity as a function of cycle number. c) The electrochemical impedance spectra of the pristine solid-state C-S/Li_6PS_5Cl/Li-In cell and after 20 cycles.

4. Conclusions

The excellent Li-ion conductor Li_6PS_5Cl, reaching an ionic conductivity of 10^{-3} S/cm at room temperature, was obtained directly from mechanical milling at room temperature with 550 rpm for 8 h. After heat-treatment at 550 °C the Li_6PS_5Cl material displays a slightly higher ionic conductivity most likely due to the improved crystallinity. CV measurements demonstrate that Li metal is not suitable as negative electrode material for the Li_6PS_5Cl based solid-state cells displaying unstable electrochemical reactions above 2.2 V vs. Li/Li^+. Also Li-Al results in poor performance as the internal resistance quickly rises upon cycling. The best candidate tested is Li-In displaying relatively good reversibility and cyclability. The pressed C-S/Li_6PS_5Cl/Li-In cell delivers initial capacities above 1300 mAh/g decreasing below 400 mAh/g after 20 cycles. Impedance indicates that the poor cyclability of the solid-state cell is mainly caused by the increase of interface resistance between the solid-electrolyte and cathode mixture during cycling most likely a consequence of the large volume changes of the Sulphur and Lithium-Indium electrodes.

Acknowledgements

The research leading to these results has received funding from the European Research Council under the European Union's

Seventh Framework Program (FP/2007-2013)/ERC Grant Agreement n. [307161] of M.W.

Appendix A. Supplementary data

Supplementary data associated with this article can be found, in the online version, at http://dx.doi.org/10.1016/j.electacta.2016.08.081.

References

[1] V. Etacheri, R. Marom, R. Elazari, G. Salitra, D. Aurbach, Energy & Environmental Science 4 (2011) 3243.
[2] J.W. Fergus, Journal of Power Sources 195 (2010) 4554.
[3] F. Mizuno, A. Hayashi, K. Tadanaga, M. Tatsumisago, Advanced Materials 17 (2005) 918.
[4] M. Murayama, N. Sonoyama, A. Yamada, R. Kanno, Solid State Ionics 170 (2004) 173.
[5] V. Thangadurai, S. Narayanan, D. Pinzaru, Chemical Society Reviews 43 (2014) 4714.
[6] J.F. Ihlefeld, P.G. Clem, B.L. Doyle, P.G. Kotula, K.R. Fenton, C.A. Apblett, Advanced Materials 23 (2011) 5663.
[7] S. Jacke, J. Song, L. Dimesso, J. Brötz, D. Becker, W. Jaegermann, Journal of Power Sources 196 (2011) 6911.
[8] C.R. Mariappan, C. Yada, F. Rosciano, B. Roling, Journal of Power Sources 196 (2011) 6456.
[9] S. Wang, L. Ben, H. Li, L. Chen, Solid State Ionics 268 (Part A) (2014) 110.
[10] N. Kamaya, K. Homma, Y. Yamakawa, M. Hirayama, R. Kanno, M. Yonemura, T. Kamiyama, Y. Kato, S. Hama, K. Kawamoto, A. Mitsui, Nat Mater. 10 (2011) 682.
[11] H.-J. Deiseroth, S.-T. Kong, H. Eckert, J. Vannahme, C. Reiner, T. Zaiß, M. Schlosser, Angewandte Chemie International Edition 47 (2008) 755.
[12] S. Boulineau, M. Courty, J.-M. Tarascon, V. Viallet, Solid State Ionics 221 (2012) 1.
[13] S. Boulineau, J.-M. Tarascon, J.-B. Leriche, V. Viallet, Solid State Ionics 242 (2013) 45.
[14] A. Manthiram, S.H. Chung, C. Zu, Advanced Materials 2015 (1980) 27.
[15] J.-W. Choi, J.-K. Kim, G. Cheruvally, J.-H. Ahn, H.-J. Ahn, K.-W. Kim, Electrochimica Acta 52 (2007) 2075.
[16] S.S. Zhang, Journal of Power Sources 231 (2013) 153.
[17] M. Wild, L. O'Neil, T. Zhang, R. Purkayastha, G. Minton, M. Marinescu, G.J. Offer, Energy & Environmental Science 8 (2015) 3477.
[18] Z. Lin, Z. Liu, N.J. Dudney, C. Liang, ACS Nano 7 (2013) 2829.
[19] M. Agostini, Y. Aihara, T. Yamada, B. Scrosati, J. Hassoun, Solid State Ionics 244 (2013) 48.
[20] M. Chen, S. Adams, J Solid State Electrochem 19 (2015) 697.
[21] R.P. Rao, S. Adams, physica status solidi (a) 208 (2011) 1804.
[22] R.P. Rao, N. Sharma, V.K. Peterson, S. Adams, Solid State Ionics 230 (2013) 72.
[23] P. Rayavarapu, N. Sharma, V. Peterson, S. Adams, J Solid State Electrochem 16 (2012) 1807.
[24] H.M. Chen, C. Maohua, S. Adams, Physical Chemistry Chemical Physics 17 (2015) 16494.
[25] H.-J. Deiseroth, J. Maier, K. Weichert, V. Nickel, S.-T. Kong, C. Reiner, Zeitschrift für anorganische und allgemeine Chemie 637 (2011) 1287.
[26] O. Pecher, S.-T. Kong, T. Goebel, V. Nickel, K. Weichert, C. Reiner, H.-J. Deiseroth, J. Maier, F. Haarmann, D. Zahn, Chemistry-a European Journal 16 (2010) 8347.
[27] L. van Eijck, L. Cussen, J. Sykora, E. Schooneveld, N. Rhodes, A.A. van Well, C. Pappas, Journal of Applied Crystallography (2016) accepted for publication.
[28] A.C. Larson, GSAS, Los Alamos National Laboratory, 2016.
[29] G.-C. Li, G.-R. Li, S.-H. Ye, X.-P. Gao, Advanced Energy Materials 2 (2012) 1238.
[30] H. Rietveld, Acta Crystallographica 22 (1967) 151.
[31] H. Rietveld, Journal of Applied Crystallography 2 (1969) 65.
[32] K. Takada, Acta Materialia 61 (2013) 759.
[33] S. Wenzel, S. Randau, T. Leichtweiß, D.A. Weber, J. Sann, W.G. Zeier, J. Janek, Chemistry of Materials 28 (2016) 2400.
[34] M. Nagao, A. Hayashi, M. Tatsumisago, Journal of Materials Chemistry 22 (2012) 10015.
[35] B. Huang, X. Yao, Z. Huang, Y. Guan, Y. Jin, X. Xu, Journal of Power Sources 284 (2015) 206.